

Multi-scale frequency separation network for image deblurring

Yanni Zhang^{1,*}, Qiang Li^{1,*}, Miao Qi¹, Di Liu¹, Jun Kong^{1,2,†} and Jianzhong Wang^{1,†}

¹ College of Information Science and Technology, Northeast Normal University, China

² Key Laboratory of Applied Statistics of MOE, Northeast Normal University, China

Abstract

Image deblurring aims to restore the detailed texture information or structures from blurry images, which has become an indispensable step in many computer vision tasks. Although various methods have been proposed to deal with the image deblurring problem, most of them treated the blurry image as a whole and neglected the characteristics of different image frequencies. In this paper, we present a new method called multi-scale frequency separation network (MSFS-Net) for image deblurring. MSFS-Net introduces the frequency separation module (FSM) into an encoder-decoder network architecture to capture the low- and high-frequency information of image at multiple scales. Then, a cycle-consistency strategy and a contrastive learning module (CLM) are respectively designed to retain the low-frequency information and recover the high-frequency information during deblurring. At last, the features of different scales are fused by a cross-scale feature fusion module (CSFFM). Extensive experiments on benchmark datasets show that the proposed network achieves state-of-the-art performance.

Introduction

The blur artifact will affect the image quality and severely degrade the performance of downstream computer vision tasks, such as video surveillance, object detection and face recognition. Therefore, accurate and efficient image deblurring techniques have attracted much attention in both academic and industrial communities.

In the early studies, most image deblurring methods focused on estimating the blurry kernel by introducing some prior information (Koh, Lee, and Yoon 2021). However, since the blur in an image may be induced by multiple reasons, image deblurring becomes a highly ill-posed problem and it is difficult to model the complex blur kernel by simple and linear assumptions.

With the development of deep learning, some deep convolutional neural networks (CNNs) have been adopted as blur kernel estimator and showed satisfied deblurring performance (Gong et al. 2017). However, these methods always need two stages (i.e. blur kernel estimation and blurry

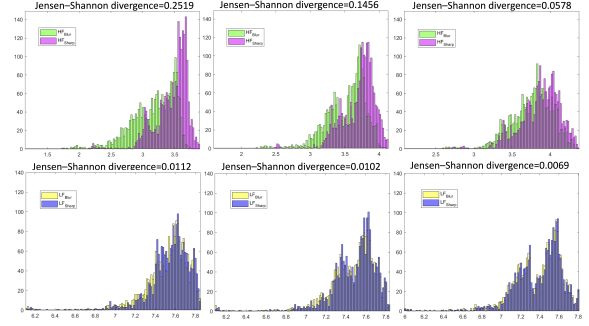


Figure 1: The distributions of entropy obtained by samples in GoPro dataset. In this figure, the LF component of each image is obtained by a low-pass Gaussian filter and the HF component is obtained by subtracting the LF component from the original image. Top: From left to right are the distributions of entropy obtained by HF components of sharp (HF_{Sharp}) and blurry (HF_{Blur}) images at original, 1/2 and 1/4 scales. Down: From left to right are the distributions of entropy obtained by LF components of sharp (LF_{Sharp}) and blurry (LF_{Blur}) images at original, 1/2 and 1/4 scales.

image deconvolution) to accomplish the image deblurring task. Therefore, they may suffer from both high computational burden and inaccurate blur kernel estimation. More recently, some other CNN based image deblurring methods were proposed to directly learn the relationship between blurry and sharp images by an image-to-image regression manner (Nah, Kim, and Lee 2017; Cho et al. 2021; Zou et al. 2021; Tao et al. 2018; Liu et al. 2020). Compared with other works, the advantage of image-to-image regression methods is that they could avoid the deblurring errors induced by inadequate blur kernel estimation. Besides, the CNN has also been combined with some other techniques such as recurrent neural network (RNN) and generative adversarial network (GAN) for image deblurring.

Although the aforementioned CNN based deblurring methods adopted various techniques to remove the blur from images, most of them leveraged the encoder-decoder architecture to capture multi-scale image features. That is, they first leverage encoder to gradually reduce the input blurry image to low-resolution representations, and then utilize de-

*Equal contribution authors. †Corresponding authors.

This work has been submitted to the IEEE for possible publication. Copyright may be transferred without notice, after which this version may no longer be accessible.

coder to progressively recover the original resolution for deblurring. This multi-scale strategy is reasonable for image deblurring because the low-resolution representations can easily capture coarse image features while the high-resolution representations are more suitable to recover fine image details. However, the differences of image information not only exist in the resolution scales but also can be reflected by different frequencies. That is, the smoothly changing structure and outline of an image are mainly described by its low-frequency (LF) component, while the fine details with rapid variations in image are usually described by its high-frequency (HF) component. Therefore, since the existing CNN based image deblurring methods dealt the image feature at each scale as a whole and neglected to distinguish image frequencies, their performance may not be optimal.

To overcome the above limitation, we propose a multi-scale frequency separation network (MSFS-Net) for image deblurring. MSFS-Net combines the multi-scale strategy with a frequency separation module (FSM) to capture different image features from both resolution scale and frequency aspects. Furthermore, different frequency information of the image is processed discriminatively in our work. Specifically, a simple cycle-consistency criterion is employed to maintain the LF features and a contrastive learning based module is proposed to progressively restore the HF features at different scales. Finally, a cross-scale feature fusion module (CSFFM) is also designed to compensate the information loss caused by the down-sampling of resolution scale and better fuse the feature of different scales. Experimental results and ablation analysis on three benchmark datasets demonstrate that with the help of frequency separation module and other components in our method, the proposed MSFS-Net can achieve state-of-the-art performance.

Our main contributions are fourfold:

- We propose a frequency separation module (FSM) to divide the image features into LF and HF components. Through embedding FSM into an encoder-decoder network architecture, our MSFS-Net can comprehensively capture image features of different frequencies and scales.
- To differentially deal with the various features, a cycle-consistency strategy and a contrastive learning module (CLM) are proposed to constrain the LF and HF features, respectively.
- We propose a cross-scale feature fusion module (CSFFM) to fuse the features of encoder and decoder from different scales, so that the multi-scale information can be better used to facilitate the deblurring.
- Extensive experiments are conducted to demonstrate the effectiveness of our proposed MSFS-Net and the modules in it.

Related Works

Image Deblurring

Nowadays, the deep CNN models with image-to-image regression strategy have been proved to be effective for image deblurring task. The pioneer work was multi-scale

CNN (MSCNN) proposed by (Nah, Kim, and Lee 2017). Inspired by MSCNN, (Gao et al. 2019) proposed a coarse-to-fine image deblurring network with selective parameter sharing and nested skip connections between different sub-networks. (Purohit and Rajagopalan 2020) adopted an encoder-decoder backbone with dense deformable and self-attention modules to improve the deblurring performance. (Cho et al. 2021) presented a multi-input multi-output U-net (MIMO-UNet) which utilized a single U-Net (i.e., encoder-decoder with short connections) but multiple input and output images to handle the coarse-to-fine image deblurring. (Chi et al. 2021) utilized an encoder-decoder network to extract multi-scale image features, and then integrated the auxiliary and meta learning to enhance the deblurring performance. (Chen et al. 2021) also applied encoder-decoder architecture to implement multi-scale and multi-stage image restoration tasks by introducing a new normalization method. In order to achieve better deblurring effect, (Zhang et al. 2018) proposed an image deblurring approach by utilizing RNN to receive different directional sequence of CNN features. (Tao et al. 2018) proposed a scale-recurrent network (SRN) by introducing the long-short term memory (LSTM) and ResBlock into an encoder-decoder based deblurring model. The success of GAN also promoted image deblurring research. (Kupyn et al. 2018) proposed a DeblurGAN to model different blur sources, in which a CNN with encoder-decoder architecture was employed as generator and a convolutional patch-based classifier was adopted as discriminator. Based on DeblurGAN, DeblurGAN-v2 (Kupyn et al. 2019) was proposed to incorporate a double-scale discriminator and a feature pyramid network into GAN to achieve better deblurring result.

Frequency Separation

An image can be decomposed into different frequency bands, and different frequency bands contain structures and textures with distinct characteristics. Therefore, analyzing the image feature in frequency domain is a commonly used technique in many conventional low-level computer vision tasks. Recently, researchers have also proposed some deep learning based deblurring methods which consider the characteristics of different image frequency. (Chakrabarti 2016; Schuler et al. 2015) employed CNN for blur kernel estimation in frequency domain. In image-to-image regression framework, (Liu et al. 2020) designed a two-stage method which first separates the HF residual information from the blurry image and then adopts an encoder-decoder network to realize the information refinement. (Zou et al. 2021) utilized discrete wavelet transform to divide the dilated convolution features into four frequency bands, so that different frequency features can be refined independently. Nevertheless, the above two methods only separated the image frequency in the first or last layer of the network. Thus, they can only capture the image features of different frequencies from a specific scale and ignored the different image frequency features of multiple scales.

Contrastive Learning

Contrastive learning (Hadsell, Chopra, and Lecun 2006) is a widely used self-supervised strategy. Motivated by the success of its application in representation learning (Komodakis and Gidaris 2018), some researchers have adopted contrastive learning to model the comparative relationships between features in computer vision tasks (Chen et al. 2020; Grill et al. 2020). Recently, (Park et al. 2020b) adopted contrastive learning in an image-to-image translation network. (Wu et al. 2021) designed a network using contrastive learning to remove the haze from hazy image. (Wang et al. 2021) also applied contrastive learning to obtain invariant degradation representation in image super-resolution problem. Although these methods demonstrated that contrastive learning can help to improve the performance of some low-level vision tasks, there are few works employ contrastive learning in image deblurring problem. Therefore, how to make good use of contrastive learning to facilitate the performance of image deblurring is still needed to be studied.

Method

Motivation

In multi-scale and hierarchical image deblurring methods, researchers have realized that the image features of different scales or spatial resolutions reflect diverse characteristics (Nah, Kim, and Lee 2017). Nevertheless, previous deblurring works seldom took the frequency information of image into consideration. In this study, we observe that the difference between blurry and sharp images lies in both the scale and frequency aspects. To justify our observation, we compare the entropy obtained by all samples with different frequencies and scales in GoPro dataset. From the distributions in Fig. 1, we can find that the discrepancy between blurry and sharp images at the same scale is mainly reflected by their HF components. Specifically, the Jensen–Shannon divergences between entropy distributions obtained by HF components of sharp and blurry images are much larger than those obtained by LF components. This phenomenon may due to that blurring can be regarded as a process of diffusing the information encoded in sharp edges across an image, which would not dramatically alter the smoothly changing structure and outline of the image (Koh, Lee, and Yoon 2021). Moreover, we can also see that the difference between entropy distributions of sharp and blurry images with large scale is greater than that with small image scale since the down-sampling will sacrifice the texture details of images.

Overview

Motivated by the observation from Fig. 1, we propose a multi-scale frequency separation network (MSFS-Net), which makes full use of different frequency features at different scales, to achieve better deblurring performance. Figure 2 shows the overall architecture of the MSFS-Net.

As can be seen from Fig. 2, the architecture of MSFS-Net is based on an encoder-decoder structure to hierarchically extract multi-scale image features. First, a blurry image is

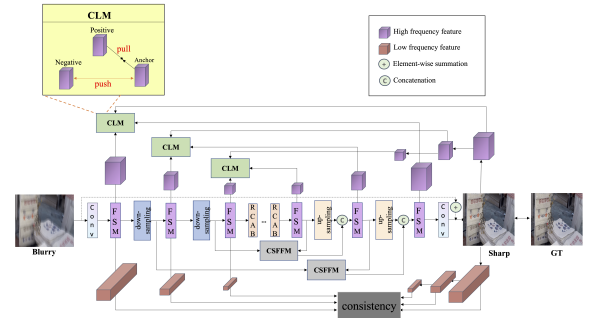


Figure 2: The architecture of the proposed MSFS-Net.

input and a 3×3 convolution is applied to get shallow features. Then, the down-sampling module and frequency separation module (FSM) are combined in the encoder stage to progressively extract the LF and HF features of image at different scales. The down-sampling module consists of 3×3 convolution with step 2 and LeakyRelu, and FSM is proposed to decompose the down-sampled features into different frequency. After the encoder stage, multiple RCABs (Shi et al. 2016) are further adopted to refine the latent feature and improve the model capacity. Next, we use up-sampling module to achieve scale restoration of features in the decoder stage. The up-sampling module consists of RCAB with pixel-shuffle (Shi et al. 2016) and FSM is also adopted to decompose the restored features at each scale. Since the decoder stage requires delicately use of fine-grained details to reconstruct features, the cross-scale feature fusion module (CSFFM) is applied to connect features at different scales of encoder and decoder stages so that different context information can be passed to each other and well preserved. In order to minimize the loss of information and make the network converge rapidly, we fuse the feature of input image with the features after the last 3×3 convolution of decoder by an element-wise summation. Last but most important, in order to take full advantage of LF and HF information, we reuse the encoder of network to obtain different frequency features of output sharp image at different scales, and two distinct strategies are carried out to constrain the LF and HF features in the intermedia layers of our network. On the one hand, since LF features of the blurry and sharp images at the same scale are similar, a simple cycle-consistency criterion is utilized to ensure that the LF features of the output sharp and input blurry images are not far away from each other. On the other hand, we propose a contrastive learning module (CLM) to regularize the HF features in the decoder stage, so that the interference of HF features in blurry image can be effectively removed. Here, it should be noted that we utilize the LF and HF components of output sharp image to constrain the intermedia features of different stages in the backbone network (i.e., LF for encoder constraint and HF for decoder constraint). This is because that the encoder is mainly used to extract context and outline information of the blurry image while the detailed information of sharp image is mostly generated by the decoder. Moreover, the cycle-consistency and CLM introduce multiple closed-loop struc-

ture in our network, which is helpful to reduce the solution space of our model (Guo et al. 2020).

Frequency Separation Module

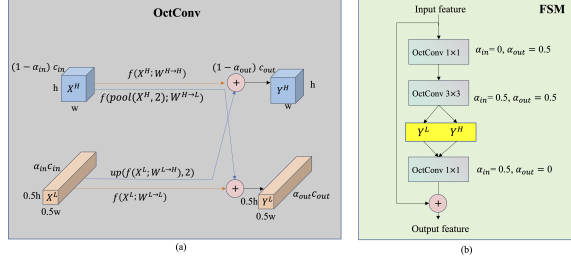


Figure 3: (a) The architecture of OctConv. (b) The architecture of frequency separation module (FSM).

Inspired by (Chen et al. 2019), Octave Convolution (OctConv) is used as the basic block of our frequency separation module (FSM). The structure of OctConv is shown in Fig. 3(a). Suppose $X \in \mathbb{R}^{c_{in} \times h \times w}$ is the input feature in which h and w denote the spatial dimensions and c_{in} is the number of channels. OctConv first decomposes X into two parts, one is HF $X^H \in \mathbb{R}^{(1-\alpha_{in})c_{in} \times h \times w}$, and the other is LF $X^L \in \mathbb{R}^{\alpha_{in}c_{in} \times 0.5h \times 0.5w}$. The parameter α_{in} adjusts the number of channels in X^H and X^L . Then, the LF and HF features are processed by convolution and the interaction between two frequencies will be carried out through pooling and up-sampling operations. The process of OctConv can be expressed by the following equations:

$$Y^H = f(X^H; W^{H \rightarrow H}) + up(f(X^L; W^{L \rightarrow H}), 2) \quad (1)$$

$$Y^L = f(X^L; W^{L \rightarrow L}) + f(pool(X^H, 2); W^{H \rightarrow L}) \quad (2)$$

where $f(X; W)$ represents the convolution with kernel W , and W is divided into W^H and W^L to convolve with X^H and X^L respectively. W^H can be further divided into $W^{H \rightarrow H}$ and $W^{L \rightarrow H}$ for intra- and inter-frequency processing. Similarly, W^L can also be divided into $W^{L \rightarrow L}$ and $W^{H \rightarrow L}$. This process can realize the communication of LF and HF information. To deal with the mismatch between spatial scales of X^H and X^L , $pool(X, 2)$ and $up(X, 2)$ are used. $pool(X, 2)$ represents average pooling with kernel size 2×2 and stride 2, and $up(X, 2)$ is an up-sampling operation by a factor of 2. Through the above operations, the output HF features $Y^H \in \mathbb{R}^{(1-\alpha_{out})c_{out} \times h \times w}$ and LF features $Y^L \in \mathbb{R}^{\alpha_{out}c_{out} \times 0.5h \times 0.5w}$ can be obtained. The parameter α_{out} is a parameter adjusts the output channels c_{out} .

Based on OctConv, the proposed FSM is shown in Fig. 3(b). First, a 1×1 OctConv ($\alpha_{in}=0$, $\alpha_{out}=0.5$) is utilized to divide the input feature into LF and HF parts. Then a 3×3 OctConv ($\alpha_{in}=0.5$ and $\alpha_{out}=0.5$) is applied to obtain the LF and HF features (denoted by Y^L and Y^H). Next, a 1×1 OctConv ($\alpha_{in}=0.5$, $\alpha_{out}=0$) is used to fuse the LF and HF features into a whole for the subsequent down-sampling or up-sampling operation. At last, a residual connection is utilized to integrate the input feature with the output of the last OctConv, so that important information is not lost in FSM.

Cross-scale Feature Fusion Module

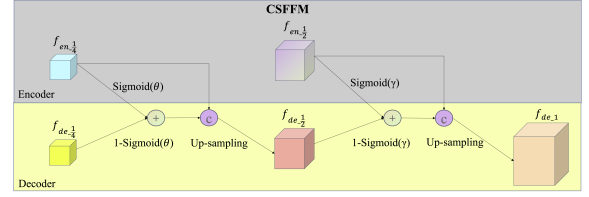


Figure 4: The architecture of the cross-scale feature fusion module (CSFFM).

From the analysis and observation in previous sections, we know that the image features with different scales exhibit different characteristics. The image feature with large scale contains fine structures such as clear edges and textures. However, with the down-sampling of feature scale, the fine structures will gradually degenerate and only the coarse structures (such as the rough contours) in the image are left. To make up for the information loss caused by down-sampling and achieve a cross-scale feature fusion, a CSFFM is proposed in our study. The CSFFM is based on the idea of adaptive mix-up operation (Zhang et al. 2017) and its specific process is shown in Fig. 4. The process can be formulated as the following equations:

$$f_{de, \frac{1}{2}} = up \left(\left[\left(\begin{array}{c} Sigmoid(\theta) * f_{en, \frac{1}{4}} \\ + (1 - Sigmoid(\theta)) * f_{de, \frac{1}{4}} \end{array} \right), f_{en, \frac{1}{4}} \right] \right) \quad (3)$$

$$f_{de, 1} = up \left(\left[\left(\begin{array}{c} Sigmoid(\gamma) * f_{en, \frac{1}{2}} \\ + (1 - Sigmoid(\gamma)) * f_{de, \frac{1}{2}} \end{array} \right), f_{en, \frac{1}{2}} \right] \right) \quad (4)$$

where $f_{en, \frac{1}{i}}$ and $f_{de, \frac{1}{i}}$ represent the features of $1/i$ scale in encoder and decoder stages (the value of i is 1, 2 and 4 in our study), θ and γ are the parameters optimizable by network, up represents the up-sampling operation and $[\]$ denotes the concatenation. CSFFM not only realizes the fusion of features at different scales but also connects the features of encoder and decoder, so that the important features of input image can be retained.

Contrastive Learning Module

The main idea of contrastive learning is to pull the positive paired samples together while push negative paired samples far apart in a feature space. In our study, a contrastive learning module (CLM) is proposed to regularize the HF features in decoder stage to get better restored images. According to Fig. 2, we can see that each CLM leverages three different features at the same scale to construct the positive and negative pairs for contrast. Here, we take the HF features obtained by the encoder stage, output sharp image and decoder stage as negative samples, positive samples and anchors, respectively. The reasons for this design are two-fold. First of all, the HF features in each scale of encoder stage

are mainly captured from the blurry image, so the information contained in them is unclear and undesirable. Secondly, since the output sharp image of backbone is closest to ground-truth, its HF features can be considered as guidance for the intermedia features in the decoder stage. Through the CLMs at multiple scales and the loss function associated with them, the adverse information in the HF features of blurry image can be effectively suppressed.

Loss Functions

Multi-scale Consistent Loss for Low-frequency Features

Inspired by cycle-consistency, we minimize the \mathcal{L}_1 distance between the LF features in encoder stage and those generated by the output sharp image, so that the LF features can be maintained during deblurring. Therefore, the multi-scale loss for LF features can be expressed by:

$$\mathcal{L}_{low} = \min \sum_{k=0}^2 \|f_k^{en,low} - f_k^{low}\|_1 \quad (5)$$

where k represents scale level, $f_k^{en,low}$ and f_k^{low} represent the $\frac{1}{2^k}$ scale LF features got by encoder and output sharp image. Here, we should point out that since the input blurry image and output sharp image are both decomposed into multi-scale LF and HF components by the same network, the consistent loss of LF features in Eq. (5) will lead the diversity of blurry and sharp images to be mainly reflected by their HF components at each scale, which could facilitate our contrastive learning module for HF features.

Multi-scale Contrastive Loss for High-frequency Features Considering all CLMs at different scales, the multi-scale contrastive loss (\mathcal{L}_{high}) for regularizing the HF features in our network can be expressed by the following equation:

$$\mathcal{L}_{high} = \min \sum_{k=0}^2 \frac{\mathcal{L}_1(f_k^{anchor}, f_k^{positive})}{\mathcal{L}_1(f_k^{anchor}, f_k^{negative})} \quad (6)$$

where k represents the scale level of feature, f_k^{anchor} , $f_k^{positive}$ and $f_k^{negative}$ represent the $\frac{1}{2^k}$ scale HF features obtained by decoder, output sharp image and encoder, respectively. \mathcal{L}_1 represents the \mathcal{L}_1 -distance. Minimizing Eq. (6) can pull the f_k^{anchor} and $f_k^{positive}$ together and push the f_k^{anchor} and $f_k^{negative}$ apart.

The Final Loss of MSFS-Net At last, the total loss function used to train our MSFS-Net can be defined as:

$$\mathcal{L}_{total} = \lambda_1 \mathcal{L}_{high} + \lambda_2 \mathcal{L}_{low} + \min \|I - G\|_1 \quad (7)$$

where $\lambda_1 = \lambda_2$ are set as 0.05 by experiment, I represents the output of our network and G is the ground-truth, \mathcal{L}_1 norm is applied to minimize the loss between the recovered image and ground-truth.

Comparison with Other Methods

To highlight the novelty of the proposed model, we compare MSFS-Net with some related methods. First, though the frequency separation has been adopted in some works to deal with image restoration problem such as super-resolution (Fritsche, Gu, and Timofte 2019; Li et al. 2021) and deraining (Fu et al. 2017), they only decomposed different frequency information from image features at a specific size. Thus, the LF and HF image features at different scales are neglected in them. For the methods which considered the frequency information of images in deblurring task (Zou et al. 2021; Liu et al. 2020), they either only focused on HF features or indiscriminately treated different frequency features of an image with the same strategy. Hence, they are still different from our proposed method. Besides, unlike some of the aforementioned methods that embed discrete cosine transform (DCT), discrete wavelet transform (DWT) and their inverse operations into the network for frequency analysis, the pure convolution based network architecture of our MSFS-Net can avoid information interchanges between the frequency and spatial domains, which makes the information propagate more smoothly. Second, contrastive learning has also been employed in some image-to-image regression tasks (Park et al. 2020b; Wu et al. 2021). However, these methods merely leveraged the contrastive learning to regularize the final output rather than the intermedia layers of the network. The different frequencies of multi-scale image features are ignored in them. The last technique related to our work is the perceptual loss (Johnson, Alahi, and Fei-Fei 2016) which also utilizes a multi-layer network to extract the features of network's output. Nevertheless, the differences between perceptual loss and our work are still apparent. The aim of perceptual loss is to measure the visual difference between the network's output and the ground-truth by features extracted from a pre-trained deep neural network (i.e., VGG (Simonyan and Zisserman 2014)). Hence, it cannot be adopted to constrain the features obtained by intermedia layers of backbone network. Furthermore, perceptual loss also overlooks the different frequency information of the image.

Experiments

Dataset and Implementation Details

We use the training set in GoPro dataset to train our model and the test set to validate our model. Besides, HIDE (Shen et al. 2019) and RealBlur (Rim et al. 2020) datasets are also employed to evaluate our model. GoPro dataset contains 3214 pairs of blurry and sharp images, in which the training and test sets consist of 2103 and 1111 pairs, respectively. HIDE dataset consists of 8422 pairs of blurry and sharp images and these images are carefully selected from 31 high-fps videos. RealBlur dataset consists of two subsets: RealBlur-J and RealBlur-R. For implementation details, the AdamW optimizer with parameter setting as $\beta_1=0.9$, $\beta_2=0.9$, $\epsilon=1e-8$ is used to optimize our network. The epochs and batch size are set as 3000 and 4 respectively. The initial learning rate is set as $1e-4$ and decreased by the factor of 0.5 at every 500 epochs.

Quantitative and Qualitative Evaluation

GoPro Dataset To demonstrate the effectiveness of the proposed MSFS-Net, we compare the performance of our method with some state-of-the-art algorithms on GoPro dataset. The quantitative comparison result is listed in Table 1, and some visual comparisons are shown in Fig. 5. In our experiment, the PSNR and SSIM results of all comparison methods are directly quoted from their corresponding literatures. Recently, (Chu et al. 2022) have shown that Test-time Local Converter (TLC) can effectively reduce the inconsistency of train-test information distributions and improve the performance of image restoration without any model fine-tuning. Thus, we also combine TLC with our proposed MSFS-Net (denoted as MSFS-Net-Local) to compare its deblurring performance with some improved versions of other methods.

Table 1: Performance comparison on GoPro and HIDE datasets.

Methods	GoPro		HIDE	
	PSNR	SSIM	PSNR	SSIM
DeblurGAN (Kupyn et al. 2018)	28.70	0.858	24.51	0.871
MSCNN (Nah, Kim, and Lee 2017)	29.08	0.914	25.73	0.874
(Zhang et al. 2018)	29.19	0.931	-	-
DeblurGAN-v2 (Kupyn et al. 2019)	29.55	0.934	26.61	0.875
(Yuan, Su, and Ma 2020)	29.81	0.937	-	-
DMPHN (Zhang et al. 2019)	30.21	0.935	29.09	0.924
SRN (Tao et al. 2018)	30.26	0.934	28.36	0.915
(Liu et al. 2020)	30.31	0.920	-	-
(Gao et al. 2019)	30.92	0.942	29.11	0.913
DBGAN (Zhang et al. 2020)	31.10	0.942	28.94	0.915
MT-RNN (Park et al. 2020a)	31.15	0.945	29.15	0.918
SDWNet (Zou et al. 2021)	31.26	0.966	28.99	0.957
(Whang et al. 2022)	31.66	0.948	29.77	0.922
MIMO-UNet (Cho et al. 2021)	31.73	0.951	-	-
RADN (Purohit and Rajagopalan 2020)	31.76	0.953	-	-
(Jiang et al. 2020)	31.79	0.949	-	-
(Suin, Purohit, and Rajagopalan 2020)	31.85	0.948	29.98	0.930
SPAIR (Purohit et al. 2021)	32.06	0.953	30.29	0.931
(Chi et al. 2021)	32.50	0.958	30.55	0.935
MPRNet (Zamir et al. 2021)	32.66	0.959	30.96	0.939
HINet (Chen et al. 2021)	32.71	0.959	30.33	0.932
MSFS-Net	32.73	0.959	31.05	0.941
MIMO-UNet++ (Cho et al. 2021)	32.68	0.959	-	-
HINet-Local (Chu et al. 2022)	33.08	0.962	30.66	0.936
Whang et al.-SA (Whang et al. 2022)	33.23	0.963	30.07	0.928
MPRNet-Local (Chu et al. 2022)	33.31	0.964	31.19	0.942
MSFS-Net-Local	33.46	0.964	31.30	0.943

From Table 1, we can see that the deblurring performance of our method is superior to other state-of-the-art methods. The advantage of MSFS-Net can be attributed to the following reasons. First, different from some comparison methods that only adopt a simple skip connection mechanism to concatenate the features with the same scale in encoder and decoder (Cho et al. 2021; Tao et al. 2018), the CSFFM in our model can better fuse the features of different scales and stages (i.e., encoder and decoder). Second, the methods in (Nah, Kim, and Lee 2017; Kupyn et al. 2018) integrate the

multi-scale image features by some sophisticated network structure and modules. However, they treat the image as a whole and neglect the characteristics of different image frequencies. Thus, their performance is inferior to our model which makes full use of the LF and HF information separated by FSM. At last, the method in (Liu et al. 2020) considers the frequency information in image deblurring problem. But it only focuses on the HF image features. Although SDWNet (Zou et al. 2021) utilizes the DWT for image frequency separation, it indistinguishably processes the LF and HF image features using the same network. Hence, the deblurring results of above two methods are worse than our MSFS-Net which utilizes different strategies (i.e. contrastive learning and consistent loss) to handle multi-scale HF and LF features separately. From Table 1, we can also see that TLC promotes the performance of our MSFS-Net and MSFS-Net-Local outperforms the improved versions of some other methods. Through the visual comparison in Fig. 5, the superiority of our MSFS-Net over other methods can be intuitively demonstrated.

In Fig. 6, we show the entropy distributions of LF and HF components obtained by sharp images and deblurred images of our MSFS-Net. Through comparing the results with those in Fig. 1, we can see that our proposed method can effectively narrow the gap between the sharp and blurry images. That is, the Jensen-Shannon divergencies between entropy distributions of different frequencies at each scale are much smaller than those in Fig. 1.



Figure 5: Visual comparison of the deblurring results on GoPro dataset.

HIDE and RealBlur Datasets Following some other works, we also evaluate our GoPro-trained MSFS-Net on HIDE and RealBlur datasets to test its generalization ability. From the quantitative and visual comparison results in Table 1 and Fig. 7, it can be seen that the proposed method achieves the best deblurring result on HIDE dataset. Similarly, the advantage of our MSFS-Net for handling real blurry images is justified in Table 2. Here, we should note that TLC cannot improve the performance of our GoPro trained model when it is directly applied on RealBlur dataset. This may due to the blurry images in RealBlur are captured in real scenario rather than synthesized from video. Thus, their characteristics are different from the training samples in GoPro. However, once the training of our model is conducted on RealBlur, MSFS-Net-Local outperforms the original MSFS-Net and some other methods.

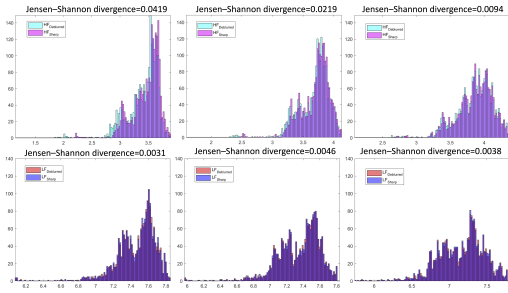


Figure 6: The distributions of entropy obtained by samples in GoPro dataset. Top: From left to right are the distributions of entropy obtained by HF components of sharp (HF_{Sharp}) and deblurred ($HF_{Deblurred}$) images at original, 1/2 and 1/4 scales. Down: From left to right are the distributions of entropy obtained by LF components of sharp (LF_{Sharp}) and deblurred ($LF_{Deblurred}$) images at original, 1/2 and 1/4 scales.

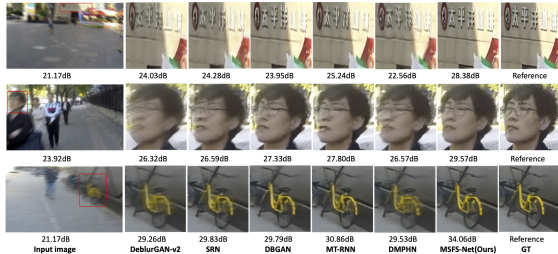


Figure 7: Visual comparison of the deblurring results on HIDE dataset.

Ablation Study and Analysis

In this section, we conduct several experiments to evaluate the effectiveness of the components proposed in our MSFS-Net. Through discarding each component in our model, we can get five new network structures (MSFS-Net w/o FSM but w/ CLM or Consistency, w/o CSFFM, w/o CLM and w/o Consistency). In order to fairly compare their performance, we use the same parameter settings to train these networks. The results of ablation experiment on GoPro dataset are shown in Table 3. First, neither CLM nor Consistency constraint can achieve satisfied deblurring result when we don't decompose the image features into different frequency by FSM. On the one hand, the energy of an image is mostly concentrated in its LF components. Thus, if we neglect different frequency information and treat the image features as a whole, the contrastive loss in Eq. (6) will be dominated by the very similar LF components of blurry and sharp images. As a result, the difference between HF components of blurry and sharp images, which is very crucial for image deblurring, will be overlooked. On the other hand, imposing the Consistency constraint on the unseparated frequency features will also prevent our model from restoring the HF details during the deblurring. Second, the removal of CSFFM deteriorates the performance of our model. This is due to CSFFM can make connections between features at differ-

Table 2: Performance comparison on RealBlur dataset under two different settings: 1). applying our GoPro trained model directly on the RealBlur set. 2). Training and testing on RealBlur data where methods are denoted with symbol *.

Methods	RealBlur-R		RealBlur-J	
	PSNR	SSIM	PSNR	SSIM
MSCNN (Nah, Kim, and Lee 2017)	32.51	0.841	27.87	0.827
DeblurGAN (Kupyn et al. 2018)	33.79	0.903	27.97	0.834
DeblurGAN-v2 (Kupyn et al. 2019)	35.26	0.944	28.70	0.866
(Zhang et al. 2018)	35.48	0.947	27.80	0.847
SRN (Tao et al. 2018)	35.66	0.947	28.56	0.867
DMPHN (Zhang et al. 2019)	35.70	0.948	28.42	0.860
MIMO-UNet (Cho et al. 2021)	35.47	0.946	27.76	0.863
SDWNet (Zou et al. 2021)	35.85	0.948	28.61	0.867
MSFS-Net	36.02	0.959	28.97	0.908
MSFS-Net-Local	36.01	0.958	28.89	0.906
DeblurGAN-v2* (Kupyn et al. 2019)	36.44	0.935	29.69	0.870
SDWNet* (Zou et al. 2021)	38.21	0.963	30.73	0.896
MSFS-Net*	38.26	0.972	30.89	0.929
MSFS-Net-Local*	38.87	0.974	31.53	0.932

ent stages and scales, which results in a better information fusion. Finally, we can see that the absence of Consistency constraint or CLM for separated frequency features also has an adverse impact on the deblurring result of the proposed network. This justifies that constraining the LF and HF features in the intermediate layers with consistency criterion and contrastive learning are both important for improving the deblurring performance.

Table 3: Comparison of different ablations of MSFS-Net on GoPro dataset.

FSM	CSFFM	CLM	Consistency	PSNR	SSIM
×	✓	✓	×	30.01	0.908
×	✓	×	✓	30.13	0.910
✓	×	✓	✓	30.22	0.891
✓	✓	×	✓	31.08	0.911
✓	✓	✓	×	31.54	0.913
✓	✓	✓	✓	32.73	0.959

Conclusion

In this work, we propose a multi-scale frequency separation network (MSFS-Net) for image deblurring. In order to make the network take full advantage of the LF and HF features, we propose FSM to separate features into different frequency. At the same time, to make the features of different scales communicate with each other without losing information, CSFFM is proposed to realize feature connection. Finally, the cycle-consistency and contrastive learning strategies are designed by analyzing the different characteristics of LF and HF features between blurry and sharp images. Experiments on three datasets show that MSFS-Net achieves good results in image deblurring task.

In the future, we will incorporate some novel backbone (such as Transformer) into our network to improve its fea-

ture learning power and apply our model to other image restoration tasks (such as deraining, dehazing and denoising) to test its generalization ability.

References

- Chakrabarti, A. 2016. A neural approach to blind motion deblurring. In *European conference on computer vision*, 221–235. Springer.
- Chen, L.; Lu, X.; Zhang, J.; Chu, X.; and Chen, C. 2021. HINet: Half Instance Normalization Network for Image Restoration.
- Chen, T.; Kornblith, S.; Norouzi, M.; and Hinton, G. 2020. A simple framework for contrastive learning of visual representations. In *International conference on machine learning*, 1597–1607. PMLR.
- Chen, Y.; Fan, H.; Xu, B.; Yan, Z.; Kalantidis, Y.; Rohrbach, M.; Yan, S.; and Feng, J. 2019. Drop an octave: Reducing spatial redundancy in convolutional neural networks with octave convolution. In *Proceedings of the IEEE/CVF International Conference on Computer Vision*, 3435–3444.
- Chi, Z.; Wang, Y.; Yu, Y.; and Tang, J. 2021. Test-time fast adaptation for dynamic scene deblurring via meta-auxiliary learning. In *Proceedings of the IEEE/CVF Conference on Computer Vision and Pattern Recognition*, 9137–9146.
- Cho, S. J.; Ji, S. W.; Hong, J. P.; Jung, S. W.; and Ko, S. J. 2021. Rethinking Coarse-to-Fine Approach in Single Image Deblurring.
- Chu, X.; Chen, L.; Chen, C.; and Lu, X. 2022. Improving Image Restoration by Revisiting Global Information Aggregation. In *Proceedings of the European conference on computer vision (ECCV)*.
- Fritsche, M.; Gu, S.; and Timofte, R. 2019. Frequency separation for real-world super-resolution. In *2019 IEEE/CVF International Conference on Computer Vision Workshop (ICCVW)*, 3599–3608. IEEE.
- Fu, X.; Huang, J.; Ding, X.; Liao, Y.; and Paisley, J. 2017. Clearing the skies: A deep network architecture for single-image rain removal. *IEEE Transactions on Image Processing*, 26(6): 2944–2956.
- Gao, H.; Tao, X.; Shen, X.; and Jia, J. 2019. Dynamic scene deblurring with parameter selective sharing and nested skip connections. In *Proceedings of the IEEE/CVF Conference on Computer Vision and Pattern Recognition*, 3848–3856.
- Gong, D.; Yang, J.; Liu, L.; Zhang, Y.; Reid, I.; Shen, C.; Van Den Hengel, A.; and Shi, Q. 2017. From motion blur to motion flow: A deep learning solution for removing heterogeneous motion blur. In *Proceedings of the IEEE conference on computer vision and pattern recognition*, 2319–2328.
- Grill, J. B.; Strub, F.; Altché, F.; Tallec, C.; Richemond, P. H.; Buchatskaya, E.; Doersch, C.; Pires, B. A.; Guo, Z. D.; and Azar, M. G. 2020. Bootstrap Your Own Latent: A New Approach to Self-Supervised Learning.
- Guo, Y.; Chen, J.; Wang, J.; Chen, Q.; Cao, J.; Deng, Z.; Xu, Y.; and Tan, M. 2020. Closed-loop matters: Dual regression networks for single image super-resolution. In *Proceedings of the IEEE/CVF conference on computer vision and pattern recognition*, 5407–5416.
- Hadsell, R.; Chopra, S.; and Lecun, Y. 2006. Dimensionality Reduction by Learning an Invariant Mapping. In *2006 IEEE Computer Society Conference on Computer Vision and Pattern Recognition (CVPR'06)*.
- Jiang, Z.; Zhang, Y.; Zou, D.; Ren, J.; Lv, J.; and Liu, Y. 2020. Learning event-based motion deblurring. In *Proceedings of the IEEE/CVF Conference on Computer Vision and Pattern Recognition*, 3320–3329.
- Johnson, J.; Alahi, A.; and Fei-Fei, L. 2016. Perceptual Losses for Real-Time Style Transfer and Super-Resolution. In *European Conference on Computer Vision*.
- Koh, J.; Lee, J.; and Yoon, S. 2021. Single-image deblurring with neural networks: A comparative survey. *Computer Vision and Image Understanding*, 203: 103134.
- Komodakis, N.; and Gidaris, S. 2018. Unsupervised representation learning by predicting image rotations. *International Conference on Learning Representations (ICLR)*.
- Kupyn, O.; Budzan, V.; Mykhailych, M.; Mishkin, D.; and Matas, J. 2018. DeblurGAN: Blind Motion Deblurring Using Conditional Adversarial Networks. *IEEE*.
- Kupyn, O.; Martyniuk, T.; Wu, J.; and Wang, Z. 2019. DeblurGAN-v2: Deblurring (Orders-of-Magnitude) Faster and Better. *IEEE*.
- Li, X.; Jin, X.; Yu, T.; Sun, S.; Pang, Y.; Zhang, Z.; and Chen, Z. 2021. Learning omni-frequency region-adaptive representations for real image super-resolution. In *AAAI Press*, volume 35, 1975–1983.
- Liu, K. H.; Yeh, C. H.; Chung, J. W.; and Chang, C. Y. 2020. A Motion Deblur Method Based on Multi-Scale High Frequency Residual Image Learning. *IEEE Access*, PP(99): 1–1.
- Nah, S.; Kim, T. H.; and Lee, K. M. 2017. Deep Multi-scale Convolutional Neural Network for Dynamic Scene Deblurring. In *Computer Vision and Pattern Recognition*.
- Park, D.; Dong, U. K.; Kim, J.; and Chun, S. Y. 2020a. Multi-Temporal Recurrent Neural Networks for Progressive Non-uniform Single Image Deblurring with Incremental Temporal Training. *Computer Vision – ECCV 2020*.
- Park, T.; Efros, A. A.; Zhang, R.; and Zhu, J.-Y. 2020b. Contrastive learning for unpaired image-to-image translation. In *European Conference on Computer Vision*, 319–345. Springer.
- Purohit, K.; and Rajagopalan, A. 2020. Region-adaptive dense network for efficient motion deblurring. In *Proceedings of the AAAI Conference on Artificial Intelligence*, volume 34, 11882–11889.
- Purohit, K.; Suin, M.; Rajagopalan, A.; and Boddeti, V. N. 2021. Spatially-adaptive image restoration using distortion-guided networks. In *Proceedings of the IEEE/CVF International Conference on Computer Vision*, 2309–2319.
- Rim, J.; Lee, H.; Won, J.; and Cho, S. 2020. Real-world blur dataset for learning and benchmarking deblurring algorithms. In *European Conference on Computer Vision*, 184–201. Springer.

- Schuler, C. J.; Hirsch, M.; Harmeling, S.; and Schölkopf, B. 2015. Learning to deblur. *IEEE transactions on pattern analysis and machine intelligence*, 38(7): 1439–1451.
- Shen, Z.; Wang, W.; Lu, X.; Shen, J.; Ling, H.; Xu, T.; and Shao, L. 2019. Human-aware motion deblurring. In *Proceedings of the IEEE/CVF International Conference on Computer Vision*, 5572–5581.
- Shi, W.; Caballero, J.; Huszár, F.; Totz, J.; and Wang, Z. 2016. Real-Time Single Image and Video Super-Resolution Using an Efficient Sub-Pixel Convolutional Neural Network. *IEEE*.
- Simonyan, K.; and Zisserman, A. 2014. Very deep convolutional networks for large-scale image recognition. *arXiv preprint arXiv:1409.1556*.
- Suin, M.; Purohit, K.; and Rajagopalan, A. 2020. Spatially-attentive patch-hierarchical network for adaptive motion deblurring. In *Proceedings of the IEEE/CVF Conference on Computer Vision and Pattern Recognition*, 3606–3615.
- Tao, X.; Gao, H.; Wang, Y.; Shen, X.; Wang, J.; and Jia, J. 2018. Scale-recurrent Network for Deep Image Deblurring. *IEEE*.
- Wang, L.; Wang, Y.; Dong, X.; Xu, Q.; and Guo, Y. 2021. Unsupervised Degradation Representation Learning for Blind Super-Resolution (CVPR’2021).
- Whang, J.; Delbracio, M.; Talebi, H.; Saharia, C.; Dimakis, A. G.; and Milanfar, P. 2022. Deblurring via stochastic refinement. In *Proceedings of the IEEE/CVF Conference on Computer Vision and Pattern Recognition*, 16293–16303.
- Wu, H.; Qu, Y.; Lin, S.; Zhou, J.; Qiao, R.; Zhang, Z.; Xie, Y.; and Ma, L. 2021. Contrastive learning for compact single image dehazing. In *Proceedings of the IEEE/CVF Conference on Computer Vision and Pattern Recognition*, 10551–10560.
- Yuan, Y.; Su, W.; and Ma, D. 2020. Efficient Dynamic Scene Deblurring Using Spatially Variant Deconvolution Network With Optical Flow Guided Training. In *2020 IEEE/CVF Conference on Computer Vision and Pattern Recognition (CVPR)*.
- Zamir, S. W.; Arora, A.; Khan, S.; Hayat, M.; Khan, F. S.; Yang, M.-H.; and Shao, L. 2021. Multi-stage progressive image restoration. In *Proceedings of the IEEE/CVF Conference on Computer Vision and Pattern Recognition*, 14821–14831.
- Zhang, H.; Cisse, M.; Dauphin, Y. N.; and Lopez-Paz, D. 2017. mixup: Beyond empirical risk minimization. *arXiv preprint arXiv:1710.09412*.
- Zhang, H.; Dai, Y.; Li, H.; and Koniusz, P. 2019. Deep Stacked Hierarchical Multi-patch Network for Image Deblurring. *IEEE*.
- Zhang, J.; Pan, J.; Ren, J.; Song, Y.; and Yang, M. H. 2018. Dynamic Scene Deblurring Using Spatially Variant Recurrent Neural Networks. In *2018 IEEE/CVF Conference on Computer Vision and Pattern Recognition (CVPR)*.
- Zhang, K.; Luo, W.; Zhong, Y.; Ma, L.; Stenger, B.; Liu, W.; and Li, H. 2020. Deblurring by realistic blurring. In *Proceedings of the IEEE/CVF Conference on Computer Vision and Pattern Recognition*, 2737–2746.
- Zou, W.; Jiang, M.; Zhang, Y.; Chen, L.; Lu, Z.; and Wu, Y. 2021. SDWNet: A Straight Dilated Network with Wavelet Transformation for Image Deblurring.